Supporting Information for:

Auger Recombination and Multiple Exciton Generation in Colloidal Two-Dimensional Perovskite Nanoplatelets: Implications for Light-Emitting Devices

AUTHOR NAMES. Carolina Villamil Franco[1], Benoît Mahler[2], Christian Cornaggia[1], Thomas Gustavsson[1] and Elsa Cassette[1,]*

AUTHOR ADDRESS. [1]Université Paris-Saclay, CEA, CNRS, Laboratoire Interactions, Dynamiques et Lasers (LIDYL), 91191 Gif-sur-Yvette, France. [2]Université de Lyon, Université Claude Bernard Lyon 1, CNRS, Institut Lumière Matière (ILM), F-69622 Villeurbanne, France.

* Corresponding author, email : elsa.cassette@cea.fr

Chemicals.

Lead iodide (PbI_2 99.999 %), formamidinium iodide (FA-I, anhydrous, > 99 %), n-butyl-ammonium iodide (98 %), N,N-dimethylformamide (DMF, anhydrous, 99.8 %), chloroform (anhydrous, 99 %), toluene (anhydrous, 99.8 %), acetonitrile (anhydrous, 99.8 %), ethanol (absolute, > 99.8 %), diethhylether (contains BHT as inhibitor >99.8 %) and Octadecene (ODE) were purchased from Sigma-Aldrich. Oleic acid (OA, 99 %) and 1-Octylamine (99 %) were purchased from Alfa Aesar. Oleylamine (OLAm, 90 %), Oleylamine (OLAm, 90%) and Hydriodic acid (57 wt % aqueous solution for analysis, distilled, unestabilized) were purchased from Acros Organics. Formamidinium acetate (FA-acetate), Methylamoninium iodide (MA-I, anhydrous, > 99 %), cesium iodide (Cs-I, anhydrous, > 99%), n-butyl-ammonium iodide (C_4-I, 98 %), n-octyl-ammonium iodide (C_8-I, 98 %) and dodecyl ammonium iodide (C_{12}-I) were purchased from Solar Cells.

Oleylamonium iodide (C_{18}-I) was prepared as previously reported by Kovalenko and co..[1]

Colloidal synthesis.

Hybrid perovskites nanoplatelets with controlled number of monolayers (*n=2* and *n=3*) were synthesized by injecting a fresh mixture of the precursor solutions (*L*-I: C_4-I/C_{18}-I, PbI_2 and A-I: MA-I/FA-I/Cs-I), all three dissolved separately at 0.5 M in DMF of a precise ratio, in toluene at room temperature, under vigorous stirring.

For *n=2* NPLs ($L_2[APbI_3]PbI_4$) A=MA, FA, Cs, the stoichiometric ratio employed was 2:2:1 (C_{18}I:PbI_2:A-I) so the precursor mixture was prepared with 20 µL of C_{18}-I 0.5 M solution and 20 µL of the 0.5 M PbI_2 solution and 10 µL of the A-I solution. Separately, OLAm (20 µL, 0.5 M in toluene) is added to 10 mL of toluene. Then, 20 µL of the precursor mixture was quickly injected in the toluene solution under vigorous stirring. We found that the stability of the

prepared NPLs was improved by adding this excess of ligands in the synthesis without dissolving the sample.

For MAPI *n=3* NPLs (L_2 $[MAPbI_3]_2PbI_4$), similar protocol was employed but using a stoichiometric ratio for the precursor solution of 1.5:0.5:2:2 with 15 µL of solution C_4-I, 5 µL of C_8-I solution, 20 µL of the PbI_2 solution and 20 µL of the MA-I solution. To prevent from the formation of *n*=2 NPLs, the OLAm solution is added after the injection of the precursors.

The obtained nanoplatelets dispersed in toluene were used as it (unless specified) or diluted by adding slowly toluene to reach the desired optical density (below 0.1 for TR-PL experiments and below 0.3 for TA).

Transmission electron microscopy (TEM).

The shape and size of the prepared colloidal perovskite nanostructures were determined by transmission electronic microscopy (TEM) using a JEOL 2100 equipped with a LaB_6 filament and operating at 200 kV. The results are displayed in **Figure S1** with the histograms of the measured sizes (extracted from ImageJ program) and representative pictures in inset. Minimum electron flux was used to limit the damages under the electron beam (degradation with recrystallization of PbI_2 seen as black dots on the NPL surface). The thickness of the thin nanoplatelets was deduced from their first excitonic transition energy (see main text).

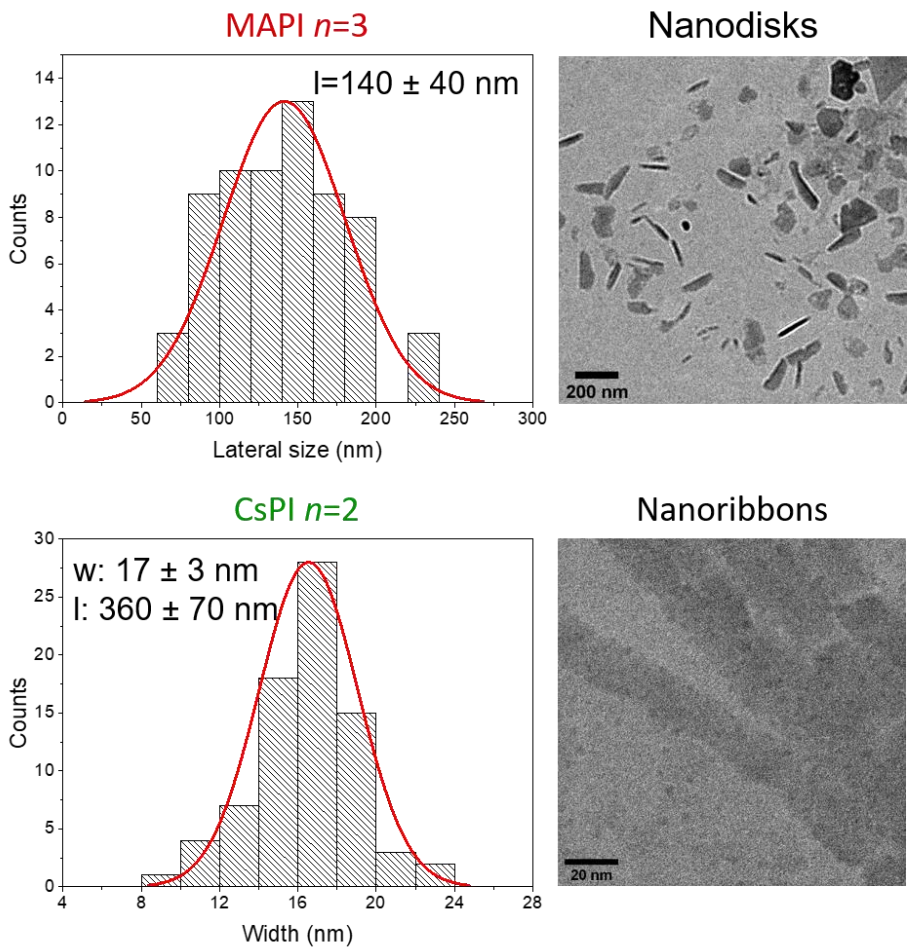

Figure S1. Histogram of the size distributions of the sample extracted from the TEM images. Legend: l = length, w = width.

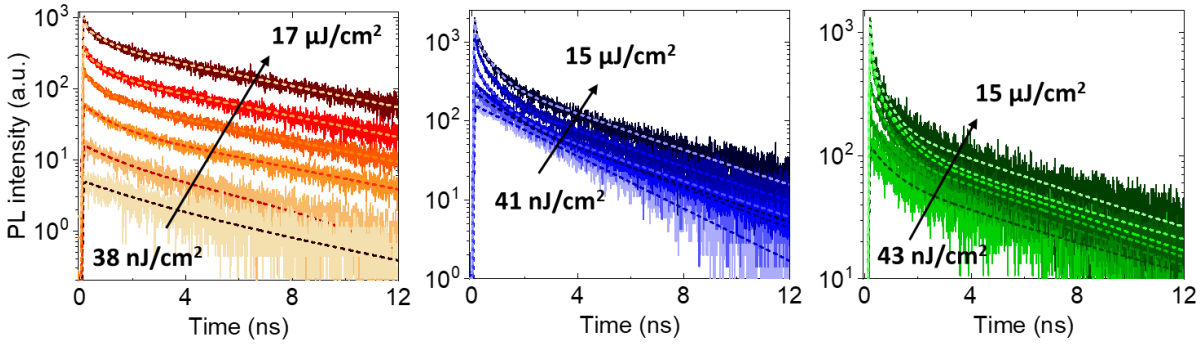

Figure S2. Fluence-dependent PL decay traces of MAPI, FAPI and CsPI *n=2* NPLs excited at 400 nm (band-edge detection). Experimental data are displayed in full lines and fit in dashed lines.

Tables S1-S4: Fit parameters for a triexponential decay of the photoluminescence at different excitation fluence for the different samples (**Table S1**) MAPI *n*=3 NPLs, (**Table S2**) MAPI *n*=2 NPLs, (**Table S3**) FAPI *n*=2 NPLs and (**Table S4**) CsPI *n*=2 NPLs.

Table S1. MAPI *n*=3 NPLs

J (μJ/cm^2)	ñ (cm^{-2})	A_1	τ_1 (ps)	A_2	τ_2 (ns)	A_3	τ_3 (ns)
0.037	8.96×10^{8}	-	-	4 ± 2	3.4 ± 0.3	2 ± 2	11 ± 7
0.11	2.66×10^{9}	-	-	4.4 ± 0.7	2.5 ± 0.4	14.6 ± 0.8	10.8 ± 0.5
0.73	1.76×10^{10}	-	-	33.2 ± 0.7	1.54 ±0.06	93.3 ± 0.8	10.5 ± 0.1
2.02	4.86×10^{10}	120 ± 3	365 ± 17	114 ± 3	1.91 ± 0.06	213.0 ± 0.6	[10.4 ± 1]*
4.94	1.19×10^{11}	374 ± 6	244 ± 9	232 ± 5	1.78 ± 0.05	387 ± 1	[10.4 ± 1]*
15.11	3.63×10^{11}	820 ± 40	50 ± 2	326 ± 3	1.42 ± 0.02	543 ± 1	[10.4 ± 1]*

*[fixed values]

Table S2. MAPI *n*=2 NPLs

J (μJ/cm^2)	ñ (cm^{-2})	A_1	τ_1 (ps)	A_2	τ_2 (ps)	A_3	τ_3 (ns)
0.038	1.03×10^{9}	-	-	60 ± 2	870 ± 52	57 ± 2	6.5 ± 0.2
0.115	3.13×10^{9}	-	-	128 ± 2	675 ± 19	99 ± 1	6.05 ± 0.08
0.777	2.10×10^{10}	208 ± 5	191 ± 8	184 ± 5	952 ± 23	114.7 ± 0.9	6.05 ± 0.05
2.28	6.16×10^{10}	467 ± 6	95 ± 3	320 ± 4	704 ± 10	120.7 ± 0.8	[6.05 ± 0.05]*
5.79	1.57×10^{11}	640 ± 11	128 ± 5	281 ± 9	840 ± 28	122 ± 1	[6.05 ± 0.05]*
17.4	4.72×10^{11}	1034 ± 25	60 ± 2	412 ± 9	552 ± 12	152 ± 1	[6.05 ± 0.05]*

*[fixed values]

Table S3. FAPI *n*=2 NPLs

J (μJ/cm^2)	ñ (cm^{-2})	A_1	τ_1 (ps)	α_2	A_2 (ps)	A_3	τ_3 (ns)
0.041	2.36×10^{9}	-	-	-	-	158.5 ± 0.5	2.62 ± 0.01
0.109	6.25×10^{9}	-	-	109 ± 3	970 ± 41	126 ± 4	3.74 ± 0.07
0.661	3.77×10^{10}	-	-	157 ± 1	847 ± 10	144 ± 1	3.39 ± 0.02
1.98	1.13×10^{11}	248 ± 5	81 ± 3	317 ± 2	676 ± 6	139.7 ± 0.5	[3.5 ± 1] *
4.98	2.84×10^{11}	775 ± 14	67 ± 2	609 ± 6	571 ± 6	209 ± 1	[3.5 ± 1] *
14.87	8.51×10^{12}	1566 ± 25	59 ± 1	876 ± 8	520 ± 6	344 ± 2	[3.5 ± 1] *

*[fixed values]

Table S4. CsPI *n*=2 NPLs

J (μJ/cm^2)	ñ (cm^{-2})	A_1	τ_1 (ps)	A_2	τ_2 (ps)	A_3	τ_3 (ns)
0.043	2.90 ×10^9	-	-	55 ± 1	729 ± 34	63.5 ± 0.6	5.9 ± 0.7
0.108	7.25 ×10^9	-	-	191 ± 2	667 ± 18	153.3 ± 0.8	6.0 ± 0.8
0.706	4.73 ×10^{10}	-	-	636 ± 3	537 ± 4	258.8 ± 0.9	5.9 ± 0.1
1.94	1.30 ×10^{11}	922 ± 11	122 ± 6	645 ± 8	787 ± 42	246 ± 1	[5.9 ± 1] *
5.00	3.35 ×10^{11}	1044 ± 20	93 ± 3	582 ± 19	684 ± 12	156 ± 1	[5.9 ± 1] *
15.02	1.01 ×10^{12}	1276 ± 21	57 ± 2	423 ± 8	526 ± 11	253 ± 3	[5.9 ± 1] *

*[fixed values]

Calculation of the excitation fluences and exciton density.

The excitation fluence in μJ/cm^2 is:

$$J = \frac{E_{pulse}}{\Sigma_{laser}}$$

where E_{pulse} is the pump energy per pulse and $\Sigma_{laser} = \pi(\omega_0)^2$ is the section of the pump laser beam with a beam waist ω_0 at the focus position for the different wavelengths. We have $E_{pulse} = P_0/RR$ with RR, the pump repetition rate (200 kHz for TCSPC and 1.5 KHz for TA) and P_0, the average power of the excitation beam. To calculate the average photogenerated excitons per nanoplatelets $\langle N \rangle$, the following expression is used:

$$\langle N \rangle = j\sigma_{abs}$$

with j the photon fluence per pulse expressed in photons/cm^2, calculated by dividing J by the energy hν of a single photon. The absorption cross section of the sample σ_{abs} at specific wavelength in cm^2 was estimated as follows:

σ_{abs} at 400 nm was estimated using previous reports of colloidal $FAPbI_3$[2] and $CsPbI_3$[3] nanocrystals or using the linear absorption coefficient of MAPI[4] taking into account that away from the confinement effects, the absorption cross section scale linearly with the nanoparticle volume.[5,6] We use the TEM measurement to determine the volume of our NPLs. Then, when

needed, the absorption cross section at other wavelengths are calculated by using the ratio of the absorption values.

Finally, the exciton density in cm^{-2} is given by $\tilde{n}=<N>/S_{NPL}$, where S_{NPL} is the surface of the NPL. The exciton density is the important parameter to take into account for the AR rather than $<N>$, as it defines the relative distance between excitons $d_{X\text{-}X} = 1/\sqrt{(\tilde{n})}$. Given that $<N>$ is proportional to σ_{abs} and this later parameter scales with the volume of the NPL: $V_{NPL} = S_{NPL} \times d_{NPL}$ (away from confinement effect, with d_{NPL} the NPL thickness, the linear absorption coefficient α_{abs} in cm^{-1} is the scaling factor between σ_{abs} and V_{NPL}), $\tilde{n}$ is independent on S_{NPL}. Thus, calculation of $\tilde{n}(0)$ is not affected by the dispersion of the NPL lateral sizes. An example of calculation is given for MAPI n=3 NPLs in **Table S5**.

P (μW)	**E_{pulse} (nJ)**	**J ($\mu J/cm^2$)**	**j (#photons/cm^2)**	**<N> (#excitons)**	**ñ (#excitons/cm^2)**
0.56	0.003	0.036	7.17×10^{10}	0.2	1.29×10^{9}
1.66	0.008	0.11	2.13×10^{11}	0.6	3.83×10^{9}
11.01	0.06	0.7	1.41×10^{12}	3.9	2.54×10^{10}
30.4	0.15	1.9	3.89×10^{12}	11	7.01×10^{10}
74.2	0.37	4.7	9.50×10^{12}	26	1.71×10^{11}
227	1.14	14.5	2.91×10^{13}	81	5.24×10^{11}

Table S5. Calculation of the excitation fluence and exciton density of MAPI n=3 NPLs in TR-PL experiments (excitation 400 nm).

Comparison of the long time TR-PL component.

The fluorescence quantum yield (QY) of the different samples Φ_S was estimated using standard reference dyes using the following formula:

$$\Phi_s = \Phi_{ref} \frac{I_s A_{ref} n_s^2}{I_{ref} A_s n_{ref}^2} \qquad \textbf{(Equation S1)}$$

with Φ_{ref}, the known PL QY value of the reference standard used; A_{ref} and A_s, the absorption value at the excitation wavelength of the reference and the sample, respectively; n_{ref} and n_s, the refractive index corresponding to the respective solvent and I_{ref} and I_s, the measured integrated fluorescence intensity of the reference and sample, respectively.

We found a PL QY of about 30 %, 10 %, 9 % and 20 % for MAPI *n*=3 NPLs, MAPI, FAPI and CsPI *n* =2 NPLs, respectively. While shorter radiative single exciton recombination rate is expected for thinner NPLs with larger exciton binding energy, the longer τ_3 component associated to MAPI *n*=3 NPL sample is essentially linked with its larger PL QY.

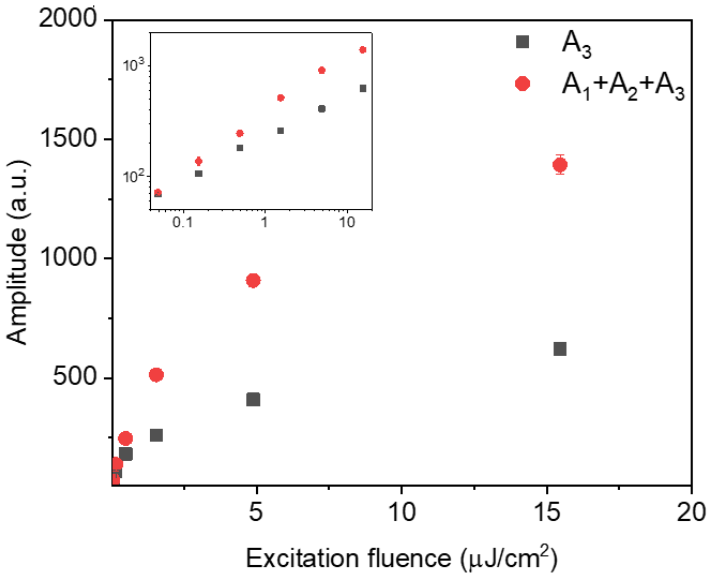

Figure S3. Evolution of the total (A_1+A_2+A_3, red dots) and single-exciton (A_3, black dots) amplitude of the time components used in the multi-exponential fit of the TR-PL decay traces of MAPI *n*=3 NPLs, for different excitation fluences. Inset: same graph in the log-log scale.

Auger recombination as the main multiexciton dynamics.

As the multiexciton time constants (τ_1 and τ_2) extracted from the fit are on the order of hundreds to tens of ps, they correspond to non-radiative AR rather than radiative biexcitonic recombination. Indeed, the radiative biexciton lifetime ($\tau_{BX,rad}$) is related to the radiative single exciton lifetime ($\tau_{X,rad}$) according to the equation [7]:

$$\tau_{BX,rad} \approx \frac{1}{2}\tau_{X,rad} = \frac{1}{2}\frac{\tau_X}{PL\ QY}$$

where $\tau_x = \tau_3$ is the measured luminescence mono-exciton lifetime and PL QY is the photoluminescence quantum yield of the sample.

By taking the long time component of the PL decay τ_x = 10.0 ± 0.8 ns and PL QY = 0.31 (measured with cresyl violet in methanol as a reference) of the *n=3* NPL sample, we found $\tau_{BX,rad} \approx 8$ ns, which is more than one order or magnitude longer than the observed time range of the multiexciton dynamics.

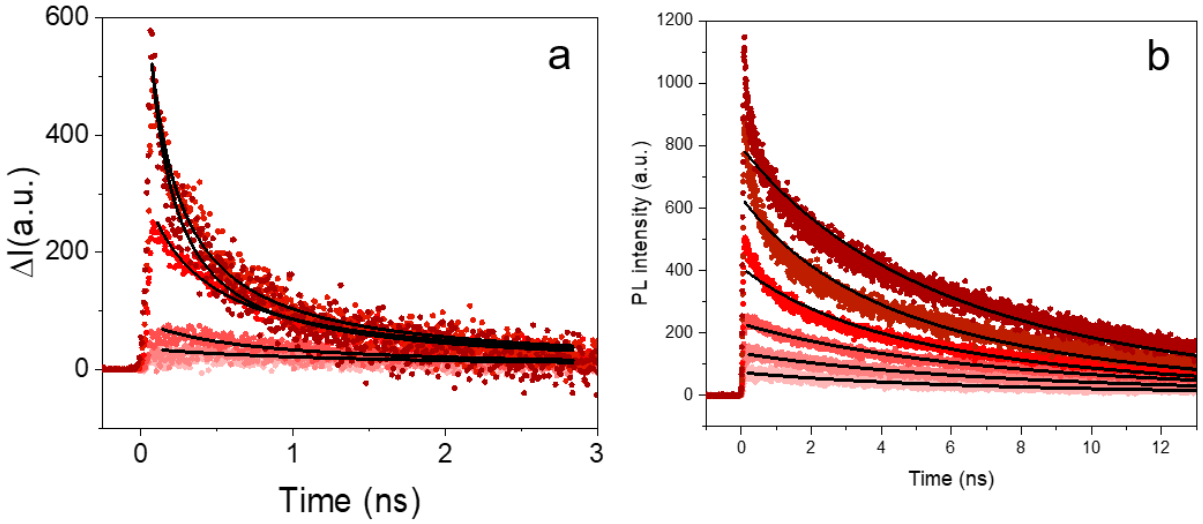

Figure S4. (a) Isolated multiexciton PL dynamics of MAPI *n*=3 NPLs excited at 400 nm with increasing excitation fluence (from light to dark red dots) and fit using a pure bimolecular dynamic (black lines, using **Equation 2**) **(b)** Full TR-PL decay traces with a fit using the mono- and bi-molecular recombination kinetics (using the **Equation S2** displayed in the legend of **Table S6**).

$\tilde{n}_0$ (cm^{-2})	β (cm^2/s) from isolated multi-exciton dynamics	β (cm^2/s) from the full TR-PL decay traces
1.29×10^9	-	2.04×10^{-2}
3.83×10^9	8.21×10^{-2}	5.2×10^{-3}
2.54×10^{10}	5.57×10^{-2}	1.89×10^{-3}
7.01×10^{10}	3.31×10^{-2}	1.38×10^{-3}
1.71×10^{11}	2.40×10^{-2}	4.9×10^{-4}
5.24×10^{11}	1.10×10^{-2}	7.9×10^{-5}

Table S6. Bimolecular AR rate extracted from the fit of the TR-PL decay traces of MAPI *n*=3 NPLs excited at 400 nm using the isolated multiexciton dynamics or the full data. We use ω_0 = 50 µm, σ_{abs} (400 nm) = 2.77 ×10^{-12} cm^2 with V_{NPL} = 2.8 ×10^{-17} cm^3 (S_{NPL} = 1.5 ×10^{-10} cm^2 and the thickness is 1.8 nm) and the linear absorption coefficient α(400 nm) = 10^5 cm^{-1} for the calculation of $\tilde{n}(0)$. Its value was fixed for the fit using **Equation 2**. For the full TR-PL decay fit, we also fixed τ_3 in the formula: $\tilde{n}(t) = \frac{\tilde{n}(0)exp(-t/\tau_3)}{1+\tilde{n}(0)\beta\tau_3[1-exp(-t/\tau_3)]}$ (**Equation S2**).

The fit of the full TR-PL decay trace of MAPI n=3 NPLs using the **Equation S2** does not reproduce the early-time dynamics associated with multiple excitons very well. The low excitation fluence data and long-time dynamics corresponding to non-interacting excitons present (at low exciton density) are however fairly well represented and give a bimolecular rate β that decreases from 2×10^{-2} to 8×10^{-5} cm^2/s with increasing excitation fluence. These values are comparable to the β-values of 5×10^{-4} and 5×10^{-3} cm^2/s reported by Delport *et al.* and *Deng et al.* respectively.[4,8] From our point of view, these values do not represent the multiexciton AR rates. They may be partially related to the presence of free carriers implying bimolecular electron-hole recombination.[9] We should also note that these values are highly dependent on the initial value of $\tilde{n}(0)$ and τ_X, which make it difficult to physically interpret the results. We thus decided to fit only the isolated multiexciton dynamics, after subtraction of the low fluence trace, using a simplified equation describing pure bimolecular dynamics (**Equation 2**).

The fact that the β-values decrease with the exciton density shows that the temporal dependency of β reduces the kinetic order of the **Equation 1**. In contrast, an increase of the β-values would have instead suggested a higher order dynamics, such as trimolecular three-particle AR involving free charge carriers, which is not the case here.

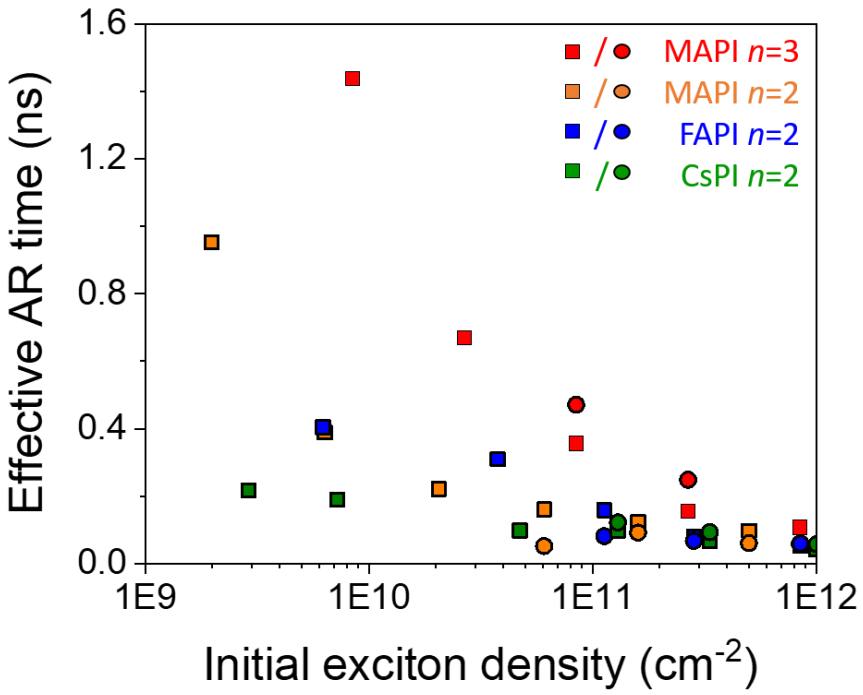

Figure S5. Effective Auger recombination time of the different perovskite NPL samples extracted from the bimolecular fit of the TR-PL decay (squares) and τ_1 extracted from the multiexponential fit (dots).

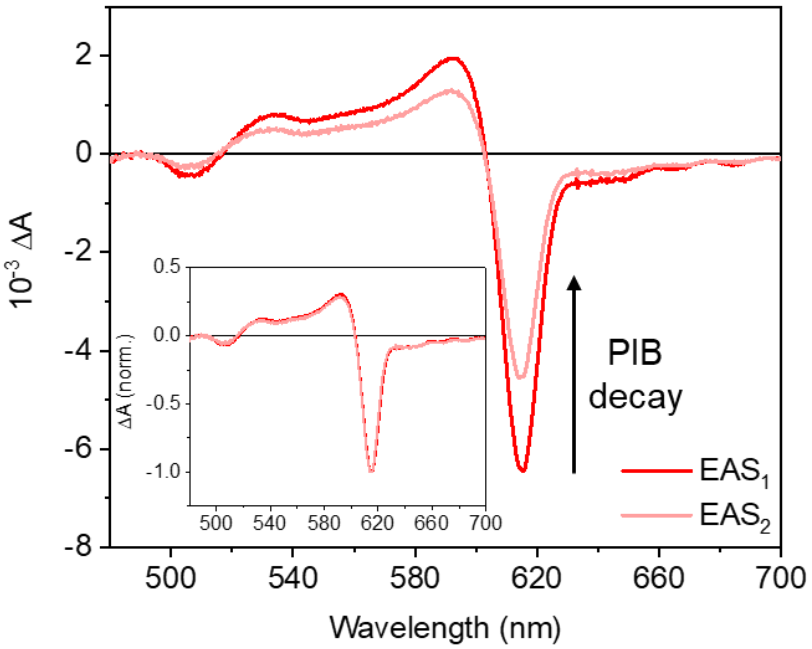

Figure S6. Evolution Associated Spectra (EAS) extracted from global analysis of MAPI *n*=3 NPLs excited at 620 nm. The exponential decay time constants are 314 ps (EAS_1 to EAS_2) and 2.4 ns (amplitude decay of EAS_2). As EAS_1 and EAS_2 are only different in amplitude (same normalized lineshape in the inset), the decay dynamics are only due to depopulation.

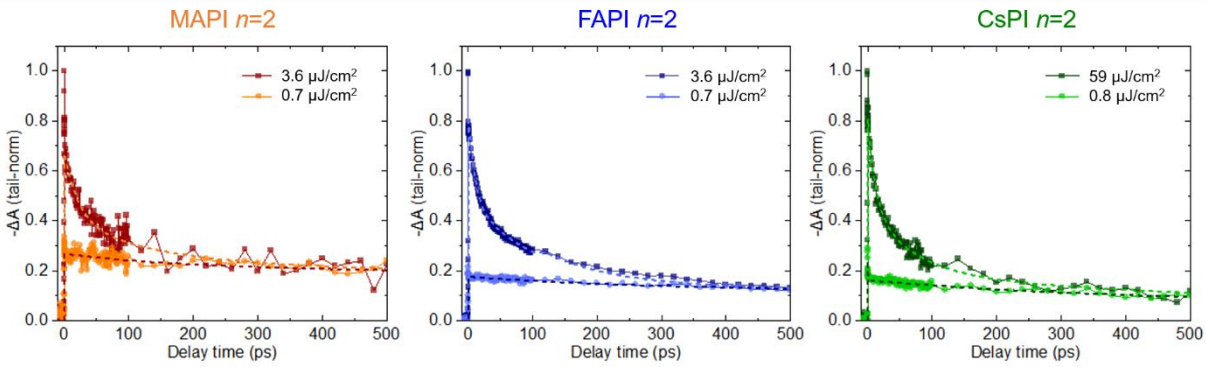

Figure S7. Band-edge PIB traces of MAPI, FAPI and CsPI *n*=2 NPLs normalized at long time for high and low excitation fluences (squares) and multiexponential fit (dashed lines).

Table S7-S10. Fit parameters for a triexponential decay of the PIB at different excitation density for (Table S7) MAPI *n*=3 NPLs, (Table S8) MAPI *n*=2 NPLs, (Table S9) FAPI *n*=2 NPLs and (Table S10) CsPI *n*=2 NPLs.

Table S7. MAPI *n*=3 NPLs

J (μJ/cm^2)	ñ (cm^{-2})	A_1	τ_1 (ps)	A_2	τ_2 (ps)	A_3	τ_3 (ns)
0.6	5.37×10^{10}	-	-	-	-	0.82 ± 0.03	11 ± 1
1.3	1.07×10^{11}	-	-	0.55 ± 0.01	259 ± 20	0.23 ± 0.01	4.5 ± 0.3
2.5	2.15×10^{11}	0.18 ± 0.09	35 ± 14	0.40 ± 0.08	155 ± 43	0.35 ± 0.02	5 ± 1
7.0	6.44×10^{11}	0.28 ± 0.03	8 ± 2	0.10 ± 0.02	95 ± 13	0.29 ± 0.07	9 ± 24
25	2.15×10^{12}	0.41 ± 0.03	11 ± 1	0.30 ± 0.02	126 ± 24	0.25 ± 0.02	5 ± 1

Table S8. MAPI *n*=2 NPLs

J (μJ/cm^2)	ñ (cm^{-2})	A_1	τ_1 (ps)	A_2	τ_2 (ps)	A_3	τ_3 (ns)
0.7	3.10×10^{10}	-	-	0.12 ± 0.01	171 ± 64	0.50 ± 0.01	[6.0 ± 1.5]*
3.6	1.80×10^{11}	6 ± 2	21 ± 9	4 ± 2	141 ± 13	5.6 ± 0.5	[6.0 ± 1.5]*

*[fixed values]

Table S9. FAPI *n*=2 NPLs

J (μJ/cm^2)	ñ (cm^{-2})	A_1	τ_1 (ps)	A_2	τ_2 (ps)	A_3	τ_3 (ns)
3.6	5.68×10^{11}	25 ± 2	9 ± 1	25 ± 1	106 ± 11	10.8 ± 0.4	[3.9 ± 0.5]*
0.7	1.14×10^{10}	-	-	0.41 ± 0.07	198 ± 1	1.71 ± 0.08	[3.9 ± 0.5]*

*[fixed values]

Table S10. CsPI *n*=2 NPLs

J (μJ/cm^2)	ñ (cm^{-2})	A_1	τ_1 (ps)	A_2	τ_2 (ps)	A_3	τ_3 (ns)
59	1.90×10^{13}	14.8 ± 0.4	8.42 ± 1	7.8 ± 0.4	316 ± 50	1.4 ± 0.3	[6 ± 1] *
0.8	2.44×10^{11}	0.31 ± 0.02	0.52 ± 0.09	0.29 ± 0.01	328 ± 42	0.32 ± 0.01	[6 ± 1] *

*[fixed values]

P (μW)	J (μJ/cm^2)	E_{pulse} (nJ)	<N> (#excitons)	ñ (cm^{-2})
1	0.6	0.7	3	2.25×10^{10}
2	1.3	1.3	7	4.49×10^{10}
4	2.5	2.7	9	6.07×10^{10}
12	7	8	28	1.82×10^{11}
18	11	12	42	2.73×10^{11}
40	25	26.7	93	6.07×10^{11}

Table S11. Calculated exciton density for the visible TA experiments in MAPI *n*=3 NPLs excited at bandedge. We use $\omega_0 = 186 \pm 5$ μm, σ_{abs} (620 nm) = 1.21×10^{-12} cm^2.

Calculation of the exciton density at 250 nm excitation.

We used a reduced excitation power (< 1 μW, < 0.7 nJ) leading to an excitation fluence of less than 3.8 μJ/cm^2. The optical density at 250 nm was less than twice the value at the bandedge (610 nm, see absorption spectrum **Figure S8**), and thus leads to an absorption cross section of about 3.5×10^{-12} cm^2 at 250 nm. The exciton density is thus 1×10^{11} cm^{-2} at maximum, corresponding to a minimum average inter-exciton distance of about 30 nm.

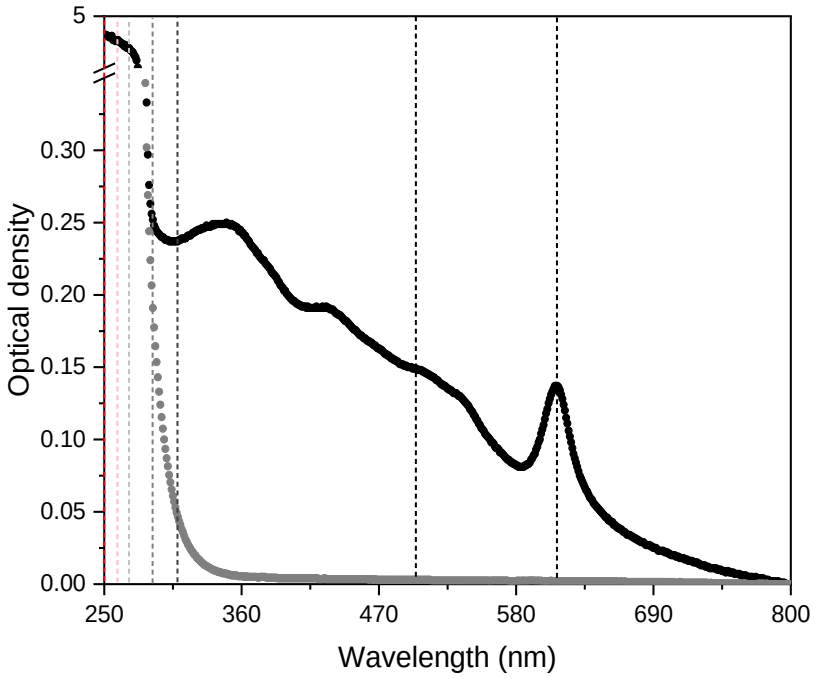

Figure S8. Absorption spectrum of MAPI *n*=3 NPLs dispersed in toluene (in black), together with the spectrum of the neat toluene (in grey). The different excitation energies used in the TA measurements are shown in dashed lines (the color scheme matches with the one used in **Figure 5a** and **S9**). The optical density at the band-edge is 0.137 and 0.211 at 400 nm. While the strong absorption from the solvent (toluene) below 290 nm prevents from determining the accurate optical density of the NPL sample at these shorter wavelengths, the gradual increased absorption towards shorter wavelengths allows to estimate a maximum absorption of 0.28 at 250 nm. It should be noted that the simultaneous increase of the light scattering in energy leads to an overestimated value of the optical density at 250 nm.

λ (nm)	A_1	τ_1 (ps)	A_2	τ_2 (ps)	A_3	τ_3 (ns)
250	0.26 ± 0.02	5 ± 1	0.26 ± 0.01	160 ± 27	0.41 ± 0.01	[9.5 ± 0.5] *
270	0.24 ± 0.03	3 ± 7	0.27 ± 0.05	295 ± 137	0.48 ± 0.06	[9.5 ± 0.5] *
280	-	-	0.17 ± 0.02	114 ± 30	0.72 ± 0.01	[9.5 ± 0.5] *
290	-	-	-	-	0.63 ± 0.07	[9.5 ± 0.5] *

*[fixed values]

Table S12. Fit parameters for the mono- to tri-exponential decay of the averaged PIB of MAPI *n*=3 NPLs at different excitation wavelengths.

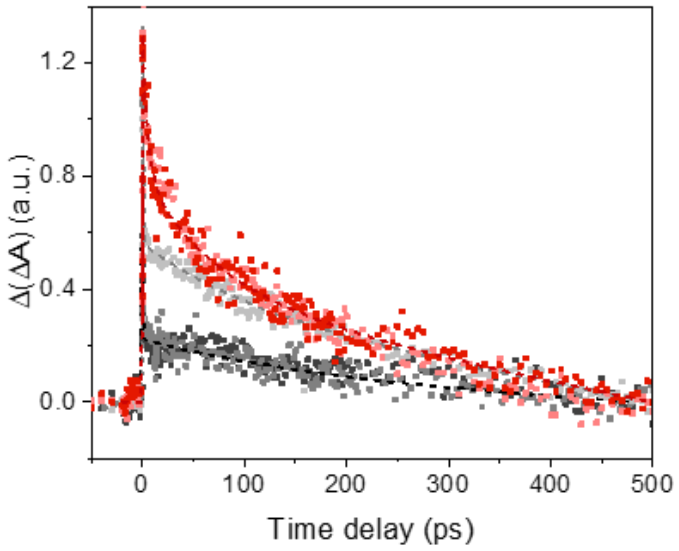

Figure S9. Isolated early-time PIB dynamics measured using UV excitation obtained by subtracting the trace acquired with visible excitation after normalization at 500 ps. Experimental data are represented by squares with the same color scheme as in **Figure 5a**.

Liquid scintillation experiments.

Liquid scintillation experiments as described previously[10] in pure toluene and in a colloidal dispersion of MAPI *n*=3 NPLs in toluene show no difference in the detected photoluminescence. This is interpreted as the absence of efficient energy transfer from the toluene molecules to the NPLs.

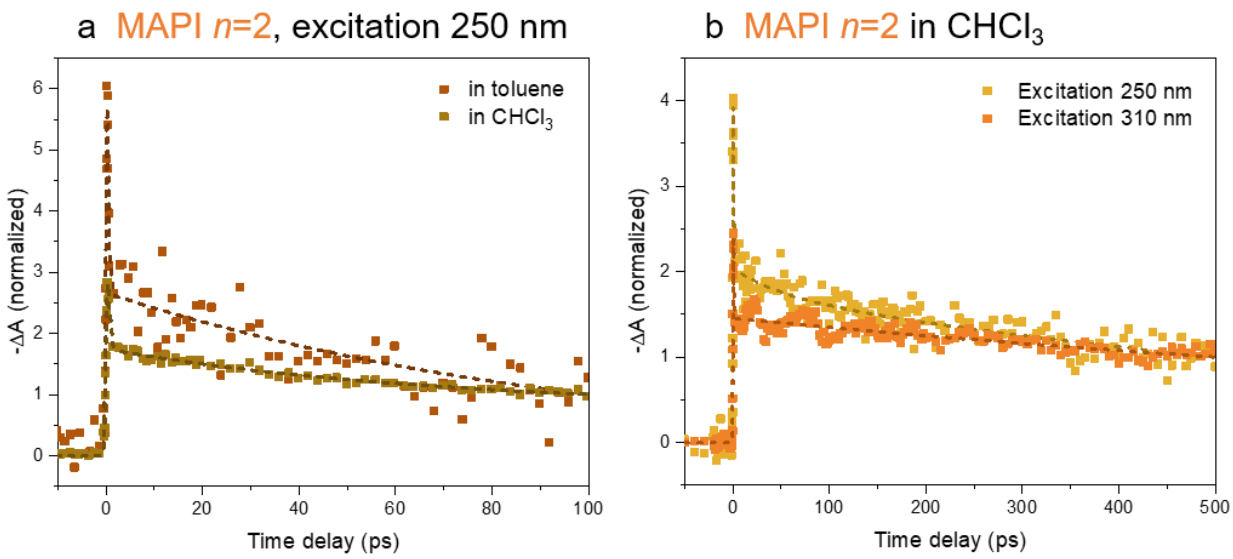

Figure S10. (a) Comparison of the PIB traces (normalized at 100 ps) of MAPI *n*=2 NPLs synthesized in toluene and chloroform measured after excitation at 250 nm with identical fluences. The traces could be fit by a coherent artifact (< 400 fs for UV experiments) and an exponential function with time component(s) of about 100 ps for the NPLs in toluene and 60 and 640 ps for the NPLs in chloroform. **(b)** PIB traces (normalized at 500 ps) of MAPI *n*=2 NPLs synthesized in $CHCl_3$ for excitation at 250 and 310 nm. Except from the coherent artifact (< 400 fs), the fit displays time components in about 50 ps and 900 ps for 250 nm excitation and 1.3 ns for 310 nm.

REFERENCES

(1) Protesescu, L.; Yakunin, S.; Kumar, S.; Bär, J.; Bertolotti, F.; Masciocchi, N.; Guagliardi, A.; Grotevent, M.; Shorubalko, I.; Bodnarchuk, M. I.; Shih, C. J.; Kovalenko, M. V. Dismantling the "Red Wall" of Colloidal Perovskites: Highly Luminescent Formamidinium and Formamidinium–Cesium Lead Iodide Nanocrystals. *ACS Nano* **2017**, *11* (3), 3119–3134. https://doi.org/10.1021/acsnano.7b00116.

(2) Fang, H.-H.; Protesescu, L.; Balazs, D. M.; Adjokatse, S.; Kovalenko, M. V.; Loi, M. A. Exciton Recombination in Formamidinium Lead Triiodide: Nanocrystals versus Thin Films. *Small* **2017**, *13* (32), 1700673. https://doi.org/10.1002/smll.201700673.

(3) Puthenpurayil, J.; Cheng, O. H. C.; Qiao, T.; Rossi, D.; Son, D. H. On the Determination of Absorption Cross Section of Colloidal Lead Halide Perovskite Quantum Dots. *J. Chem. Phys.* **2019**, *151* (15), 154706. https://doi.org/10.1063/1.5126039.

(4) Deng, S.; Shi, E.; Yuan, L.; Jin, L.; Dou, L.; Huang, L. Long-Range Exciton Transport and Slow Annihilation in Two-Dimensional Hybrid Perovskites. *Nat. Commun.* **2020**, *11* (1), 1–8. https://doi.org/10.1038/s41467-020-14403-z.

(5) Maes, J.; Balcaen, L.; Drijvers, E.; Zhao, Q.; De Roo, J.; Vantomme, A.; Vanhaecke, F.; Geiregat, P.; Hens, Z. Light Absorption Coefficient of CsPbBr3 Perovskite Nanocrystals. *J. Phys. Chem. Lett.* **2018**, *9* (11), 3093–3097. https://doi.org/10.1021/acs.jpclett.8b01065.

(6) Puthenpurayil, J.; Cheng, O. H. C.; Qiao, T.; Rossi, D.; Son, D. H. On the Determination of Absorption Cross Section of Colloidal Lead Halide Perovskite Quantum Dots. *J. Chem. Phys.* **2019**, *151* (15), 154706. https://doi.org/10.1063/1.5126039.

(7) Narvaez, G. A.; Bester, G.; Franceschetti, A.; Zunger, A. Excitonic Exchange Effects on the Radiative Decay Time of Monoexcitons and Biexcitons in Quantum Dots. *Phys. Rev. B - Condens. Matter Mater. Phys.* **2006**, *74* (20), 205422. https://doi.org/10.1103/PhysRevB.74.205422.

(8) Delport, G.; Chehade, G.; Lédeé, F.; Diab, H.; Milesi-Brault, C.; Trippé-Allard, G.; Even, J.; Lauret, J. S.; Deleporte, E.; Garrot, D. Exciton-Exciton Annihilation in Two-Dimensional Halide Perovskites at Room Temperature. *J. Phys. Chem. Lett.* **2019**, *10*

(17), 5153–5159. https://doi.org/10.1021/acs.jpclett.9b01595.

(9) Herz, L. M. Charge-Carrier Dynamics in Organic-Inorganic Metal Halide Perovskites. *Annu. Rev. Phys. Chem.* **2016**, *67* (1), 65–89. https://doi.org/10.1146/annurev-physchem-040215-112222.

(10) Broda, R.; Cassette, P.; Kossert, K. Radionuclide Metrology Using Liquid Scintillation Counting Related Content. *Metrologia* **2007**, *44* (4), S36. https://doi.org/10.1088/0026-1394/44/4/S06.